Surface and Catalytic Elucidation of Rh/gamma-Al2O3 Catalysts during NO Reduction by C3H8 in the Presence of Excess O-2, H2O, and SO2

ARTICLE *in* THE JOURNAL OF PHYSICAL CHEMISTRY A · OCTOBER 2009

Impact Factor: 2.69 · DOI: 10.1021/jp907589c · Source: PubMed

Surface and Catalytic Elucidation of $Rh/\gamma\text{-}Al_2O_3$ Catalysts during NO Reduction by C_3H_8 in the Presence of Excess O_2, H_2O, and SO_2[†]

G. Pekridis,[‡] N. Kaklidis,[‡] V. Komvokis,[§] C. Athanasiou,[§] M. Konsolakis,[||] I.V. Yentekakis,[||] and G. E. Marnellos*[,‡,§]

Department of Mechanical Engineering, University of Western Macedonia, Bakola & Sialvera, GR-50100 Kozani, Greece, Chemical Process Engineering Research Institute, Centre for Research & Technology Hellas, sixth km. Charilaou - Thermi Road, P.O. Box 361, GR-57001 Thermi, Thessaloniki, Greece, and Laboratory of Physical Chemistry and Chemical Processes, Department of Sciences, Technical University of Crete, GR-73100 Chania, Crete, Greece

Received: August 6, 2009; Revised Manuscript Received: October 2, 2009

The present study aims at exploring the surface and catalytic behavior of $Rh/\gamma\text{-}Al_2O_3$ catalysts during the selective reduction of NO by C_3H_8 in the presence of excess oxygen, H_2O, and SO_2 with particular emphasis on identifying the elementary steps that describe the reaction mechanism. To this end, detailed activity and stability tests were employed and a precise kinetic analysis was carried out at differential conditions to elucidate the effect of each reactant, including H_2O and SO_2, on the total reaction rate. At the same time, temperature programmed desorption (TPD) studies in combination with in situ diffuse reflectance infrared Fourier transform (DRIFT) spectroscopy were carried out under various reaction conditions to correlate the catalytic performance of $Rh/\gamma\text{-}Al_2O_3$ catalyst with its corresponding surface chemistry. The results reveal that in the absence of H_2O and SO_2, the reaction follows a typical "reduction" type mechanism, where the active intermediates (NO_X, carboxylates, isocyanates) are interacting to yield the final products. In this reaction sequence the formation of carboxylate ($C_xH_yO_z$) species is considered as the rate determining step. Water affects in a different way the NO and C_3H_8 conversion performance of $Rh/\gamma\text{-}Al_2O_3$ catalyst; its effect is totally reversible in the case of C_3H_8 oxidation, while the NO reduction was permanently affected mainly due to the oxidation of Rh active sites. In contrast, SO_2 poisons both reactions irreversibly via the formation of strongly adsorbed sulfate compounds, which hinder the adsorption and consequently the activation of reactants.

1. Introduction

Abatement of nitrogen oxides (NO_X) emissions from stationary and mobile sources consists of a subject of considerable interest, since NO_X contribute significantly to a variety of emerged environmental issues, such as the formation of photochemical smog and acidification, affecting the quality of the atmosphere and therefore human health, flora, fauna and materials.[1] Nowadays, the three-way catalytic converters (TWCs) comprise a well established technology for automotive pollution control under stoichiometric conditions,[2−4] whereas the method of selective catalytic reduction of NO_X by ammonia (NH_3−SCR) is employed as the best choice at stationary applications.[1,4]

Lean burn gasoline and diesel engines both operating under oxygen excess conditions (lean burn conditions) offer significantly fuel economy and notably lower CO_2 emissions.[5] However, under these oxidative conditions the use of TWCs is limited by their inability to reduce effectively NO_X to N_2.[3] On the other hand, in stationary sources, problems related with the storage and slip of ammonia, urge the development of new catalytic systems capable of removing NO_X emissions at the effluent of flue gases.[6]

The selective catalytic reduction of NO_X by hydrocarbons (HC-SCR) has received considerable attention as an effective technology for NO_X abatement both from lean burn engines and stationary sources, since hydrocarbons coexist with NO_X in flue gases. As a result, employing this particular method can successfully yield the simultaneous control of NO_X and hydrocarbons emissions in a single device.[1,4] This candidate process was first studied over zeolite catalysts under oxygen excess conditions, resulting in high deNO_X activity over a wide temperature range.[5,7] However, several disadvantages of zeolites related mainly to their poor hydrothermal stability and their low activity in the presence of H_2O and SO_2, limits their use for practical applications.[3−5] Metal oxides have been also studied for the HC-SCR, demonstrating high activity and hydrothermal stability,[3,8] but low tolerance to SO_2 poisoning.[9,10] Among the catalysts studied for HC-SCR, noble metal supported catalysts are the most promising candidates, showing high efficiency for NO_X reduction and relatively enhanced resistance to SO_2 and H_2O poisoning.[3,4] Platinum supported catalysts are the most active at low temperatures, exhibiting, however, high selectivity toward the undesirable N_2O.[11,12] Rhodium-containing catalysts exhibit satisfactory activity at relatively high temperatures but display superior selectivity to N_2, consisting one of the most promising catalysts for the SCR of NO_X by hydrocarbons at lean conditions.[11,12]

Due to the high activity of noble metals and their enhanced tolerance against SO_2 and steam presence, considerable efforts have been dedicated to the elucidation of the HC-SCR reaction mechanism.[3,13,14] Although there is no general agreement about

[†] Part of the special issue "Green Chemistry in Energy Production Symposium".

* To whom correspondence should be addressed. Tel.: +30 2461 0 56690. Fax: +30 2461 0 56601. E-mail: gmarnellos@uowm.gr.

[‡] University of Western Macedonia.

[§] Centre for Research & Technology Hellas.

[||] Technical University of Crete.

10.1021/jp907589c
Published on Web 10/23/2009

the precise prevailing reaction mechanism due to the complexity of intermediate steps, two general schemes could be proposed for this process. The first one, the so-called "decomposition" mechanism, involves the dissociative adsorption of NO on metal active sites as a first step, followed by the recombination of adsorbed N_{ad} to produce gas phase N_2.[3,4,13,14] According to this scheme the role of the reducing agent is to scavenge the catalyst surface from oxygen ad-atoms thus keeping the metal entities in reduced state; the oxidation state of noble metals seems to be of crucial importance for NO dissociation since only the reduced sites are considered to be active for this process.[15−18] In line with the second general scheme for the HC-SCR, the "reduction" mechanism consists of complex surface interactions between adsorbed NO_X species and surface hydrocarbons' fragments, where as a result various reaction intermediates, such as cyanide (−CN) and isocyanate (−NCO) species are produced.[3,4,13,14]

In spite of the numerous spectroscopic and/or kinetic studies devoted to the SCR of NO,[1,3,4,13,14] only a few of them are dealing with the use of propane (C_3H_8) instead of propene (C_3H_6) as a reducing agent, although the former is one of the major constituents among the hydrocarbons emitted from mobile or stationary sources.[19] This reductant (C_3H_8) is expected to exhibit different surface and catalytic behavior, compared to C_3H_6, due to their different adsorption strength on the surface of noble metals.[19−21] In addition, none of the above studies deals with the surface chemistry modifications induced by the presence of SO_2 and/or H_2O, although the latter coexist in the exhaust stream of real de-NO_X processes. These molecules significantly alter the overall catalytic activity and thus it is of critical importance to realize their specific role on the surface and consequently on the catalytic behavior.

In the present study we investigate the SCR of NO by C_3H_8 over Rh/γ-Al_2O_3 catalysts under excess oxygen conditions in either the presence or absence of SO_2 and H_2O, giving particular emphasis on the reaction mechanism elucidation. To this direction, detailed activity and stability tests along with a precise kinetic analysis are performed under differential conditions to determine the apparent reaction orders and activation energies. Temperature programmed desorption (TPD) measurements in combination with in situ diffuse reflectance infrared Fourier transform spectroscopic (DRIFTS) studies were also carried out under various reaction conditions to correlate the samples' catalytic performance with their surface chemistry.

2. Experimental Section

2.1. Materials. The dry impregnation technique was used to synthesize rhodium supported on γ-Al_2O_3 catalysts with nominal loading of 1.0 wt %. Initially, γ-Al_2O_3 extrudates (Engelhard) were crushed and sieved to obtain a fraction of particles with size 180−355 μm. The impregnation of the support with Rh was performed using a $RhCl_3 \cdot 3H_2O$ solution provided by Alpha Products. The catalyst was then dried at 120 °C for 2 h and calcined at 600 °C for 6 h under stagnant atmospheric air. The heating rate in all stages was kept constant at 10 °C/min.

2.2. Catalyst Characterization. The total surface area of the 1% Rh/γ-Al_2O_3 catalyst was determined by nitrogen physical adsorption/desorption experiments at −196 °C using an Autosorb-1 (Quantachrome) flow apparatus by applying the Brunauer−Emmett−Teller (BET) method and was found equal to 186 ± 0.20 m^2/g, slightly lower compared to the BET surface area of bare alumina (204 ± 0.25 m^2/g). For metal loading determination the inductively coupled plasma atomic emission spectroscopy (ICP/AES) was used, resulting in Rh loading of 10250 ± 400 ppm.

2.3. Reaction/Analysis System. The experimental setup employed for the catalytic measurements consists of the feed unit, the reactor and the gas analysis network.[22] Reactant gases included NO/He, O_2/He, C_3H_8/He, and SO_2/He mixtures and He of 99.999% purity and were all supplied by Air Liquide. Water was introduced into the reactor by bubbling the reacting mixture through a vessel containing liquid water, at ambient temperature. The feed unit was equipped with flow controllers and pressure indicators for the accurate control of the flow and partial pressure of each reactant. The experiments were carried out in a quartz fixed-bed catalytic microreactor (0.008 m i.d.). The catalyst was loaded onto a fine-quartz fritted disk and the reaction temperature was continuously monitored by a thermocouple.

Reactants and products analysis was performed with a series of online gas analyzers and a gas chromatograph (SHIMADJU 14B) equipped with a thermal conductivity detector (TCD). A molecular sieve 13X column (10 ft × $^1/_8$ in.) was used to separate oxygen, nitrogen and carbon monoxide, while a porapack QS column (10 ft × $^1/_8$ in.) was employed for the nitrous oxide, propane, and carbon dioxide separation. Water concentration was always calculated by applying hydrogen and oxygen mass balances. The online analyzers were a chemiluminesence $NO/NO_2/NO_X$ analyzer (2020 Enviromax, Liston Scientific) and nondispersive infrared (NDIR) CO_2 (ANARAD), CO (MIRAN 203), and SO_2 (ROSEMOUNT NGA 2000) analyzers.

The typical feed composition employed during light-off (200−600 °C) and stability (410 °C) tests was 0.13% NO, 5% O_2, 0.17% C_3H_8, 0−400 ppm SO_2, and 0−3% H_2O balanced with He. The total gas flow rate was 100 cm^3 (STP)/min, and the weight of catalyst was 0.2 g, corresponding to a *W*/*F* and GHSV values equal to 0.12 (g·s)/mL and 20000 h^{-1}, respectively. Prior to each experiment, the catalytic samples were heated in He flow (600 °C/1 h/120 cm^3 min^{-1}) to eliminate possible residue from the metal precursor and to ensure stable operation.

2.4. Temperature Programmed Desorption Procedure. To evaluate the NO_X sorption capacity over both the support (γ-Al_2O_3) and 1%Rh/γ-Al_2O_3 catalysts, temperature programmed desorption (TPD) studies were performed in the same quartz U-tube reactor, loaded with 0.2 g of fresh catalyst using a total flow rate of 100 cm^3/min. The catalyst prior to TPD procedure was initially pretreated under pure He flow at 600 °C for 1 h. Then it was cooled at the adsorption temperature (410 °C). At this temperature the reactor was fed for 1 h by a gas mixture consisting of one or more of the following constituents: 0.13% NO, 5% O_2, 0.17% C_3H_8, 100 ppm SO_2, 3% H_2O diluted in He. Then, the reactor was cooled at 100 °C and the feed was switched to pure He for 1 h to desorb the physically adsorbed species. The temperature was then increased to 600 °C using a heating rate of 10 °C/min. The exit of the reactor was connected to the gas analysis system, and the variation of NO_X and SO_2 concentrations were recorded continuously with the temperature.

2.5. FT-IR Procedure. Diffuse reflectance IR studies were performed in an Excalibur FTS 3000 spectrometer, equipped with an MCT detector cooled by liquid nitrogen and a high temperature environmental IR chamber (Specac, Environmental Chamber DRIFT model) designed for in situ sample treatment. Spectra were obtained using a resolution of 2 cm^{-1} with accumulation of 64 scans. During these measurements the external optics were purged with CO_2-free dry air generated from an air purifier system (Claind Italy, CO_2-PUR model). The

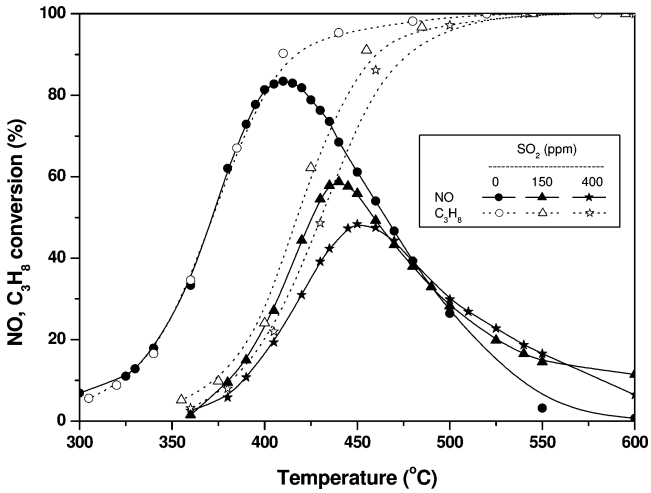

Figure 1. Effect of SO_2 concentration on NO and C_3H_8 conversion profiles over Rh/Al_2O_3 catalyst. Reaction conditions: 1300 ppm NO, 1700 ppm C_3H_8, 5% O_2, 0−150−400 ppm SO_2 in He; W/F = 0.12 g s cm^{-3}.

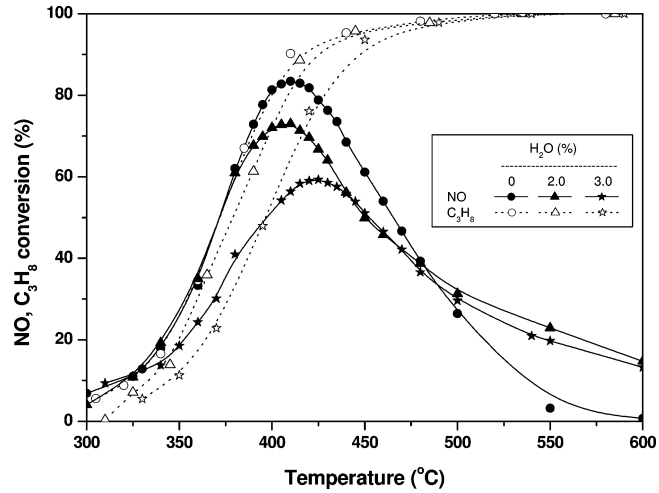

Figure 2. Effect of H_2O concentration on NO and C_3H_8 conversion profiles over Rh/Al_2O_3 catalyst. Reaction conditions: 1300 ppm NO, 1700 ppm C_3H_8, 5% O_2, 0−2.0−3.0% H_2O in He; W/F = 0.12 g s cm^{-3}.

catalytic sample (∼80 mg), in a powder form, was placed in the IR chamber, and its surface was flattened to optimize the intensity of reflected beam. The IR chamber was supplied by the appropriate gas mixtures. The total flow rate through the IR cell was maintained at 80 cm^3/min and before each experiment the catalytic sample was pretreated as follows: (i) oxidation at 500 °C with 20.7% O_2 for 30 min, (ii) purging with He flow at 500 °C for 30 min, and (iii) temperature decrease under He flow and background spectra acquisition at the desired temperatures.

Three different set of DRIFTS experiments were performed in the present study:

(i) Time evolution of adsorbed species experiments at room temperature and constant feed composition.

(ii) Steady-state experiments under a constant feed composition in the interval of 200−470 °C.

(iii) Transient experiments involving at first exposure of catalyst surface to a certain gas mixture and then a switch to another mixture to investigate the reactivity of preadsorbed species.

3. Results and Discussion

3.1. Effect of SO_2 and H_2O on the Activity and Stability of Rh/γ-Al_2O_3. In most cases the flue gases of combustion processes contain both SO_2 and H_2O at various concentrations. This fact implies that under real conditions a deNO_X catalyst should maintain high performance even in the presence of SO_2 and H_2O on feed stream. Therefore, the first part of the present work is dealing with the influence of SO_2 and H_2O on the activity and stability of 1% Rh/γ-Al_2O_3 catalysts.

Figure 1 presents a typical light-off experiment, where the dependence of both NO and C_3H_8 conversions on the reaction temperature (200−600 °C) is depicted under different SO_2 concentrations in the feed (0, 150, and 400 ppm). In all cases, the well-known volcano-type NO conversion profile was obtained, while C_3H_8 conversion follows a sigmoid curve approaching completion at temperatures close to NO maximum conversion. In the SO_2-free reaction mixture a maximum NO conversion of about 84% was achieved at 410 °C, whereas at the same temperature C_3H_8 consumption has been almost completed. In this point it is noteworthy to mention that such values of NO conversion are notably higher compared to corresponding ones obtained during the SCR of NO by C_3H_6 over Rh/γ-Al_2O_3 catalysts,[23] indicating the significant role of reducing agent on the NO conversion. Concerning the influence of SO_2 on catalytic activity, it is obvious from Figure 1 that SO_2 has a clear negative effect on both NO and C_3H_8 conversions. This negative effect is revealed by (i) the lower NO conversions achieved in SO_2-containing mixtures, (ii) the shifting of NO and propane conversion profiles to higher temperatures, and (iii) the progressive suppress of catalytic activity, as the SO_2 concentration is increased. Thus, in a reaction mixture containing 400 ppm of SO_2 the maximum NO conversion was 48% at 450 °C compared to 84% at 410 °C over SO_2-free gas mixtures. At the same time the C_3H_8 conversion profile has been shifted to notably higher temperatures, resulting in a C_3H_8 light-off temperature (i.e., temperature at which 50% conversion is reached) of 430 °C instead of 370 °C over SO_2-free mixtures. It should be noticed that SO_2 inhibition is not proportional to SO_2 content, since the catalytic activity suppression is more severe when the SO_2 content is in the range of 0−150 instead of 150−400 ppm. This indicates a progressive poisoning of catalyst surface that tends to stabilize at higher SO_2 concentrations; this assumption is certified below on the basis of SO_2-step changes experiments where the catalyst is periodically exposed to different SO_2 concentrations.

The corresponding results concerning the effect of H_2O concentration on the overall conversion performance are depicted in Figure 2. It is obvious that the presence of 2.0% H_2O suppresses the maximum NO conversion from 84% (in the absence of H_2O) to 73%, while when 3.0% H_2O was added in the feed stream the NO conversion was further decreased to 60%. Concerning C_3H_8 conversion, H_2O addition results in a less pronounced inhibition shifting the activity curves to higher temperatures, providing C_3H_8 light-off temperatures of about 378 and 396 °C over 2.0 and 3.0% H_2O-containing mixtures, respectively, compared to 370 °C over H_2O-free mixtures.

The durability of Rh/γ-Al_2O_3 in SO_2 and H_2O containing feed gas mixtures was investigated by step-change stability tests, where both conversions of NO and C_3H_8 were continuously monitored while the reaction feed stream was switched from SO_2- or H_2O-free to SO_2- or H_2O-containing mixtures, respectively. Figure 3 depicts the NO and C_3H_8 conversions that correspond to step changes of various SO_2 concentrations (50−500 ppm) at 410 °C. The catalyst was initially exposed to

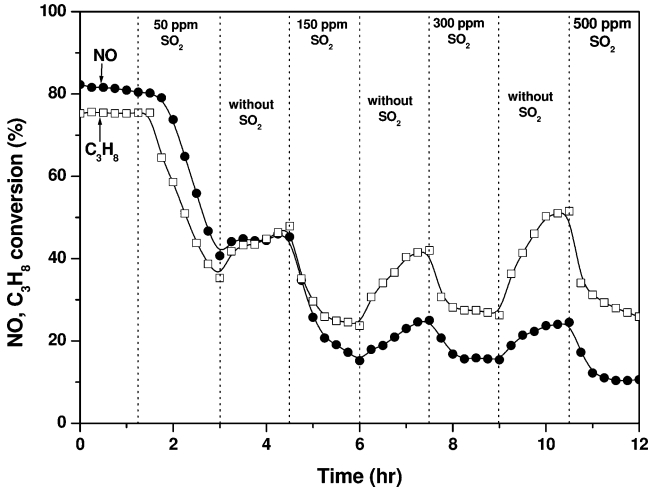

Figure 3. Effect of periodic exposure of Rh/Al_2O_3 catalyst to SO_2 containing reaction mixtures on NO and C_3H_8 conversions as a function of time on stream. Reaction conditions: 1300 ppm NO, 1700 ppm C_3H_8, 5% O_2, 0−50−150−300−500 ppm SO_2 in He; $T = 410$ °C, $W/F = 0.12$ g s cm^{-3}.

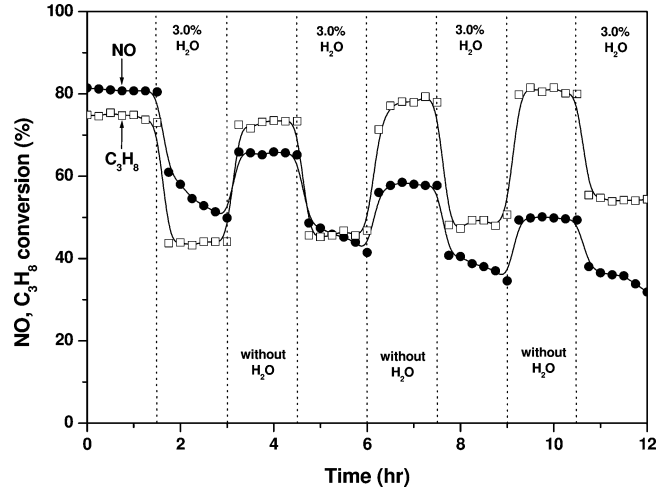

Figure 4. Effect of periodic exposure of Rh/Al_2O_3 catalyst to H_2O containing reaction mixtures on NO and C_3H_8 conversions as a function of time on stream. Reaction conditions: 1300 ppm NO, 1700 ppm C_3H_8, 5% O_2, 0−3.0% H_2O in He; $T = 410$ °C, $W/F = 0.12$ g s cm^{-3}.

a SO_2-free feed mixture for 1.5 h. In this initial step, both NO and C_3H_8 conversions were kept constant and equal to 80 and 75%, respectively. When 50 ppm of SO_2 was added in the feed mixture, NO and C_3H_8 conversions were instantaneously decreased linearly with time on stream at about 40 and 35%, respectively. Removing SO_2 from the feed slightly increased conversions to 45 and 48%, implying that the inhibition effect was irreversible. The same NO conversion behavior was observed in the sequential interchanges between SO_2-containing and SO_2-free mixtures, leading to a gradual decrease of NO conversion to values as low as 11%, in the mixture that contained 500 ppm SO_2. In all step changes, when SO_2 was removed from the feed, NO conversion was slightly increased but always to lower values compared to the previous SO_2-free gas mixture. This strong inhibition can be attributed to the gradual build up of sulphates on catalyst's surface,[3,9,22] as also revealed in the present work by DRIFTS studies over sulphated catalysts (see section 3.3).

As far as the C_3H_8 conversion is concerned, a different behavior is observed especially after the insertion of 150 ppm SO_2, where upon SO_2 removal the activity is dramatically increased. This is more obvious in the third cycle where C_3H_8 conversion tends to overcome the inhibition induced by SO_2. It can be stated that after the initial degradation occurred at 50 ppm SO_2, the effect on C_3H_8 conversion is totally reversible in contrast to the case of NO conversion. This contradiction will be explained below on the basis of the surface behavior of SO_2-treated samples.

In Figure 4, the corresponding results concerning the influence of H_2O-step changes on NO and C_3H_8 conversions are depicted. Immediately after the introduction of 3.0% H_2O on reaction feed stream, NO and C_3H_8 conversions drop suddenly to 50 and 44%, respectively, remaining then constant for the rest of the H_2O-containing cycle. Removing H_2O from the feed mixture returned propane conversion to the initial value achieved in the absence of H_2O. On the contrary, the catalytic activity for NO conversion was partly regained (66% conversion). A similar trend was observed in the next three cycles, where C_3H_8 conversion in H_2O-containing feeds was suppressed at the same steady-state range and totally recovered at the H_2O-free mixtures. Concerning the NO conversion, a progressive degradation was observed in every H_2O-containing feed step, resulting to a final NO conversion as low as 35% at the end of the fourth cycle. This indicates that H_2O has a permanent negative effect on sites related with NO reduction in contrast to that related to C_3H_8 oxidation. Taking into account that reduced Rh sites are considered as the active sites for NO reduction,[15−18] it can be proposed that the oxidation of Rh sites by H_2O adsorption[24] is responsible for the inferior NO reduction activity. In consistency with this explanation is the fact that C_3H_8 oxidation can successfully proceed over bare γ-Al_2O_3 support, in contrast to NO reduction (data not shown for brevity's sake), indicating that Rh sites are mainly responsible for NO activation.

In relative literature studies a significant deactivation by water has been observed when nonoxygenated reducing agents are employed.[3] For instance, Efthimiadis et al.[25] found that the presence of water in the feed gas stream caused a reversible inhibition over Pt-, Cu-, and Ni-alumina catalysts, attributed to the competitive adsorption between water and reactants for the same active sites.[25] Similar results were found over $Ga_2O_3-Al_2O_3$ catalysts when C1−C3 hydrocarbons were used as reducing agents.[26]

3.2. Temperature Programmed Desorption (TPD) Studies. Figure 5 shows the NO (a), NO_2 (b), and total NO_X (c) TPD spectra obtained following interaction of Rh/γ-Al_2O_3 catalyst with different reaction mixtures. For comparison reasons in Table 1 the main TPD results concerning the temperature of desorption peaks (T_{max}) as well as the amount of NO_X desorbed species and the NO_2/NO_X ratios are presented comparatively with the corresponding ones obtained over bare γ-Al_2O_3. Focusing on the case of NO adsorption over Rh/γ-Al_2O_3 two distinct desorption peaks located at 210 and 406 °C were observed (Figure 5). The low temperature (LT) peak is similar to that observed over bare γ-Al_2O_3 (Table 1) and thus should be mainly attributed to NO_X species over the support. The high temperature (HT) peak is located at 406 °C, i.e., at 66 °C lower compared to γ-Al_2O_3 support, indicating that NO_X species related with the second peak require higher temperatures to decompose or desorb in the absence of Rh. In similar NO-TPD studies performed by Efthimiadis et al.[23] over Rh/γ-Al_2O_3 catalyst using the same procedure (activated adsorption), two overlapping peaks centered at 220 and 380 °C were observed, assigned to nitrosyl and nitrate species respectively. To this end, in NO-TPD experiments carried out at room temperature over γ-Al_2O_3 support,[27] NO was the main desorption product exhibiting three

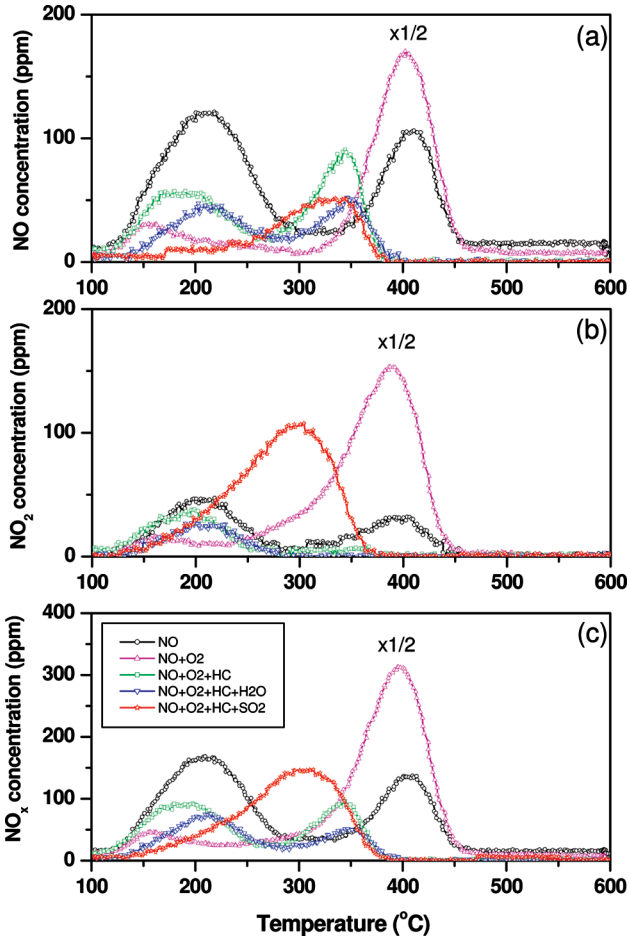

Figure 5. TPD profiles of NO (a), NO_2 (b), and NO_X (c) obtained over Rh/Al_2O_3 following interaction with the indicated gas mixtures at 410 °C for 1 h. Adsorption gases concentration: 1300 ppm NO, 1700 ppm C_3H_8, 5% O_2, 3% H_2O, 100 ppm SO_2; catalyst weight = 0.2 g; He flow rate = 100 cm^3/min; heating rate = 10 °C/min.

consecutive peaks at 100−120, 310, and 540 °C, respectively. In accordance with ref 27, the first two peaks can be assigned to nitrosyl and nitrites, whereas the high temperature peak to nitrate species. Taking into account the present results as well as the TPD studies performed over γ-Al_2O_3 supported catalysts,[23,27,28] the LT peak should be assigned to nitrosyl and nitro/nitrite species adsorbed on bare alumina and on Rh sites, whereas the HT peak to alumina−nitrate species, which could be decomposed at high temperatures to NO and to a lesser extent to NO_2 (NO_2/NO_X = 0.25). These assignments are further supported below by DRIFTS results, where it is found that nitrosyl and NO_2 species are characterized by low thermal stability.

It is worth noticing that Rh addition to γ-Al_2O_3 support significantly suppresses the NO_2/NO_X ratio on the LT peak from 0.40 to 0.25, highlighting the ability of Rh active sites to adsorb the nitrosyl species. The desorbed NO_2 can be attributed to nitro/nitrite species on alumina (generated from the oxidation of nitrosyl species by the hydroxyl groups of γ-Al_2O_3) and additionally to the oxidation of NO_{ad} with neighboring oxygen ad-atoms over Rh active sites. In contrast, the released amount of NO_X as well as the corresponding ratio of NO_2/NO_X on the HT peak, are similar to those obtained over the support, verifying the assignment of the HT peak to the decomposition of alumina nitrates.

Adding 5% O_2 to the NO/He sorption mixture shifted the position of the LT and HT desorption peaks (T_{max}) to lower temperatures, suggesting a facilitation of NO_X species desorption. At the same time the total amount of the LT desorbed NO_X from bare alumina (32.8 μmol) and Rh/alumina (18 μmol) samples were notably decreased compared to that in the absence of O_2, due to the consequent oxidation of nitrosyl and nitro/nitrite species to nitrates. This explains why the desorbed NO_X amounts in the HT peak are dramatically enhanced (107 and 124 μmol over alumina and Rh/γ-Al_2O_3, respectively) compared to O_2-free TPD experiment results. In addition, the NO_2/NO_X ratios of the LT and HT peaks remain unaffected by O_2 over alumina, while the corresponding ratios over Rh/γ-Al_2O_3 samples are increased to 0.35 and 0.5 (Table 1), respectively. This indicates, in accordance with literature,[23] that under oxidative conditions Rh sites facilitates the formation of NO_2 species.

TPD experiments were also performed under reaction conditions (NO + C_3H_8 + O_2), identical to those imposed in activity tests. As can be seen in Figure 5, the amount of NO_X species related to the LT peak is slightly increased (23.5 μmol) compared to that of NO + O_2-TPD (18 μmol), while that over γ-Al_2O_3 support remains almost constant (~33 μmol). In addition, the T_{max} of LT peak over Rh/Al_2O_3 sample is increased to 190 °C compared to 157 °C under NO + O_2-TPD. On the basis of these observations, it could be argued that propane facilitates the reduction of Rh active sites and consequently the amount and the adsorption strength of nitrosyl species. On the other hand, the amount of NO_X released at high temperatures was dramatically decreased (14.2 μmol) in the presence of propane, while that of NO_2 was completely disappeared. Taking into account that in the adsorption temperature (410 °C), NO reduction by propane proceeds at almost the maximum extent over Rh/γ-Al_2O_3 catalysts, this possibly indicates that NO_2 ad-species could be active intermediates, as indeed observed in previous studies.[16] In addition, the T_{max} of the HT peak is notably decreased by 50 °C, indicating that the presence of propane enhances NO_X desorption, while this is not the case over bare alumina where the corresponding T_{max} remained almost constant (453 °C).

Addition of H_2O in the reacting mixture results in a decrease of the desorbed amount of both LT- and HT-NO_X species from Rh/γ-Al_2O_3 catalyst (Figure 5), while a more severe suppression was observed over bare γ-Al_2O_3 (Table 1). This indicates the inhibition effect of H_2O on NO_X adsorption ability, justifying the competitive adsorption between water and NO_X ad-species for the same active sites.[25] In addition, the oxidation of Rh sites by H_2O adsorption[24] could be responsible for the inferior NO adsorption capacity, given that reduced sites are considered as the active sites for NO adsorption and consequently activation.[15−18] These observations justify the poisoning effect of H_2O, as indicated in the corresponding light-off (Figure 2) and stability (Figure 4) experiments.

In the last part of TPD experiments H_2O was substituted by SO_2 (100 ppm) to explore the NO sorption capacities of both alumina and Rh/γ-Al_2O_3 in the presence of SO_2. Over bare γ-Al_2O_3 (Table 1) the intensity as well as the T_{max} of the LT peak is decreased, implying a weakening of the adsorption strength of nitrosyl and nitro/nitrite species. On the other hand, the intensity of the HT peak and the NO_2/NO_X ratio were significantly increased. Over the Rh/Al_2O_3 sample only one NO_X peak was detected, centered at 304 °C, which is the overlapping result of the LT and mainly of HT desoprtion curves. Concurrently the desorbed amount of NO_X is higher (45.5 μmol) compared to the total released amount of NO_X (NO + NO_2) in the absence of SO_2 (37.7 μmol), while the NO_2/NO_X ratio is

TABLE 1: TPD Results at Various Reacting Mixtures over γ-Al_2O_3 and Rh/Al_2O_3 Catalysts

		NO		NO + O_2		NO + O_2 + C_3H_8		NO + O_2 + C_3H_8 + H_2O		NO + O_2 + C_3H_8 + SO_2	
		Al_2O_3	Rh/Al_2O_3	Al_2O_3	Rh/Al_2O_3	Al_2O_3	Rh/Al_2O_3	Al_2O_3	Rh/Al_2O_3	Al_2O_3	Rh/Al_2O_3
T_{max}(°C)	LT[a] peak	201	210	182	157	203	190	232	215	165	304
	HT[a] peak	472	406	454	396	453	344	481	347	456	
NO_X(μmol)	LT peak	57.3	45.9	32.8	18	33.3	23.5	18	17.7	7.8	45.5
	HT peak	28.2	24.5	107	124	45.2	14.2	10.7	8.3	64.7	
NO_2/NO_X	LT peak	0.40	0.25	0.40	0.35	0.40	0.35	0.20	0.35	0.50	0.70
	HT peak	0.25	0.25	0.25	0.50	0.15	0.00	0.00	0.00	0.50	

[a] LT: low temperature. HT: high temperature.

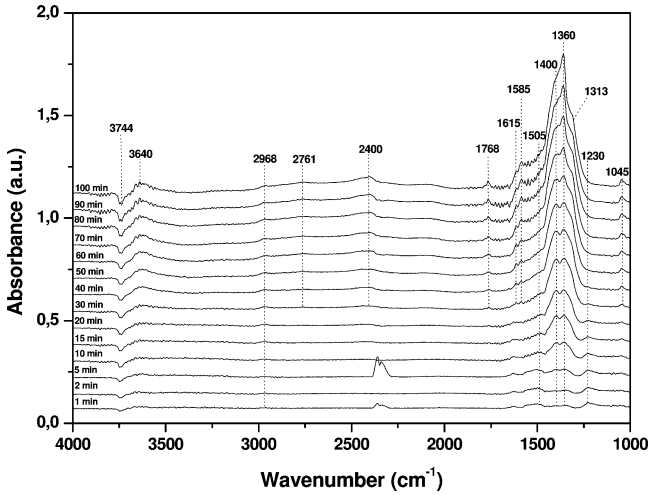

Figure 6. Time evolution of adsorbed species formed over Rh/Al_2O_3 at 27 °C under reaction conditions. FT-IR chamber feed: 1300 ppm NO, 1700 ppm C_3H_8, 5% O_2 in He; total flow rate = 80 cm^3/min.

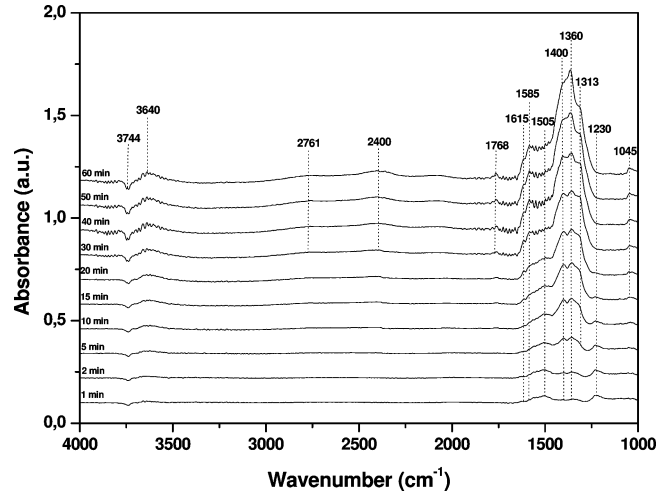

Figure 7. Time evolution of adsorbed species formed over Rh/Al_2O_3 at 27 °C during NO + O_2 adsorption. FT-IR chamber feed: 1300 ppm NO, 5% O_2 in He; total flow rate = 80 cm^3/min.

significantly increased (0.7). Taking into account the strong poisoning effect of SO_2 (Figures 1 and 3), these findings possibly indicate that SO_2 hinders the adsorption of active intermediates, such as NO and NO_2 species,[16] whereas at the same time promotes the formation of inactive nitrate species that released at high temperatures. This inhibition can be attributed to the formation of sulfates accumulated mainly on γ-Al_2O_3 support, as will be shown later on the basis of IR studies (section 3.3). It is worth mentioning that in a similar study of Efthimiadis et al.[23] it was found that in a NO + O_2 + SO_2-TPD experiment the overall amount of the desorbed NO_X was substantially higher in the absence of SO_2. This contradiction can be explained by taking into account the promotional role of SO_2 in their study[23] in contrast to the SO_2 poisoning effect observed in the present work and comes to verify the hindering role of SO_2 under the present conditions, as observed in Figures 1 and 3.

3.3. In Situ DRIFTS Studies. In situ DRIFTS experiments were carried out at temperatures in the interval of 27−500 °C, under various feed compositions (NO + C_3H_8 + O_2, NO + O_2, C_3H_8 + O_2) over Rh/γ-Al_2O_3 catalysts, to elucidate the nature and the relative population of surface species formed under steady-state reaction conditions. In each temperature the length of catalysts' exposure to gas mixture was that necessary to obtain a steady-state surface condition (constant intensity of the observed bands); usually 30−100 min depending on temperature.

Figure 6 depicts the time evolution of adsorbed species formed on the surface of Rh/γ-Al_2O_3 catalyst under NO + C_3H_8 + O_2 flow at 27 °C. Immediately after interaction of the reaction mixture with the catalyst's surface, low intensity bands at 1230, 1360, 1400, and 1505 cm^{-1} start developing. The band at 1230 cm^{-1} reaches a maximum intensity after about 10 min and then becomes weaker and finally disappears at about 30 min. After the disappearance of the band at 1230 cm^{-1}, new bands at 2761, 2400, 1768, 1615, 1585, 1313, and 1045 cm^{-1} start developing and their intensity increased with time.

Considering that under reaction conditions (NO + C_3H_8 + O_2) a number of surface species (carboxylates, carbonates, nitroxy, etc.) with overlapping bands could be copresent, the assignment of the observed bands is quite complicated. To this end, assignment is based not only on relative literature studies but also on additional IR experiments performed under NO + O_2 (Figure 7) and C_3H_8 or C_3H_8 + O_2 (Figure 8) adsorption over Rh/γ-Al_2O_3 catalysts, to elucidate the differentiation effect of nitroxy and carboxy species on the spectra acquired under reaction conditions. Comparing Figures 6−8 shows the obvious similarities of spectra obtained under NO + C_3H_8 + O_2 conditions (Figure 6) with those obtained under NO + O_2 flow (Figure 7), indicating that the dominant surface species under reaction conditions are the nitroxy species (nitro, nitrite, nitrate). This assumption is further supported by the low intensity of carboxy species (formates, acetates, carbonates, etc.) formed under C_3H_8 or C_3H_8 + O_2 adsorption (Figure 8). Thus under reaction conditions (Figure 6) the carboxy species are overlapped due to the higher intensity of nitroxy species.

On the basis of the above observations, a more precise assignment of adsorbed species could be performed. More specifically, the bands at 1230 and 1505 cm^{-1} that formed immediately after NO + O_2 (Figure 7) or NO + C_3H_8 + O_2 (Figure 6) adsorption can be assigned to nitro/nitrite species, although the band at 1505 cm^{-1} can be partially due to monodentate nitrates. The bands at 1615 and 1585 cm^{-1} that formed after the disappearance of the band at 1230 cm^{-1} are attributed to bridging and bidentate nitrates respectively, whereas the bands at 1400 and 1360 cm^{-1} are attributed to nitro

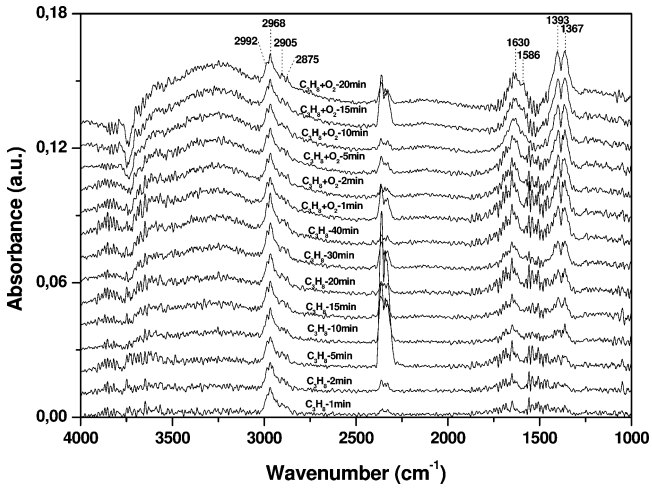

Figure 8. Time evolution of adsorbed species formed over Rh/Al_2O_3 at 27 °C during C_3H_8 or $C_3H_8 + O_2$ adsorption. FT-IR chamber feed: 1700 ppm C_3H_8 or 1700 ppm C_3H_8 + 5% O_2 in He; total flow rate = 80 cm^3/min.

compounds. The band at 1045 cm^{-1} is due to the $\nu_s(NO_2)$ vibration of bidentate nitrates, whereas the band at 1313 cm^{-1} is ascribed to the second vibration mode of nitro and/or nitrate species.[15,29,30] The bands at 2761 and 2400 cm^{-1}, which rise in parallel with the bands in the 1615−1500 cm^{-1}, could be assigned to a combination mode of nitrate species.[29,30] The disappearance of the band at 1230 cm^{-1} after about 10 min and the simultaneous evolution of the bands at 1045, 1585, 1615, 2761, and 2400 cm^{-1} reveal the transformation of nitro/nitrite species to nitrates (Figures 6 and 7). Finally, the band at 1768 cm^{-1} is attributed to the Rh−NO^- species.[18] The principal bands observed in DRIFT spectra and the corresponding assignments to surface species are summarized in Table 2.

In the O−H stretching region (Figures 6 and 7) the intensity of the negative band at 3744 cm^{-1}, characterizing isolated hydroxyl groups, is increased with time, indicating a H-bond interaction between adsorbed species and OH surface groups.[29,31] In agreement with this assumption is the development of a broadband at ~3640 cm^{-1}, characteristic of H-bonded hydroxyl groups. These findings are in accordance with the participation of OH-groups in the SCR of NO_X by propane over γ-Al_2O_3 support.[32]

Under C_3H_8 or $C_3H_8 + O_2$ adsorption (Figure 8) only weak bands at 1367, 1393, 1586, and 1630 cm^{-1} are observed and their intensity is increased with time (Figure 8). These bands are expected to overlap with the nitroxy bands formed under $NO + C_3H_8 + O_2$ conditions (Figure 6) in the same frequency region. The bands at 1586, 1393, and 1367 cm^{-1} are consistent with the bands formed during formic acid adsorption on γ-Al_2O_3 and thus are assigned to $\nu_{as}(COO^-)$, δ(CH), and $\nu_s(COO^-)$, respectively, of formate species on γ-Al_2O_3 (see ref 16 and references therein). In the C−H stretching region several bands (2992, 2968, 2905, 2875 cm^{-1}) are also observed due to gas phase propane or adsorbed hydrocarbon fragments.[16] The band at 1630 cm^{-1}, increased in parallel with the wide band at 3240 cm^{-1} can be assigned to adsorbed water.[31,33] The limited surface species formed under $C_3H_8 + O_2$ adsorption are in accordance with the lower ability of saturated or light alkanes in comparison to unsaturated hydrocarbons to generate oxygenate intermediates,[34] which are expected to have a crucial role on the SCR of NO by hydrocarbons.

To this direction, the temperature evolution of oxygenated hydrocarbon species was investigated by IR spectra acquisition under $C_3H_8 + O_2$ flow in the temperature interval of 27−400 °C, whereas the reactivity of preadsorbed oxygenated hydrocarbon species was investigated following the transient response of IR spectra after the addition of NO in the $C_3H_8 + O_2$ flow at 400 °C (Figure 9). As depicted in Figure 9 at low temperatures, the only noteworthy bands are those at 1586, 1393, and 1367 cm^{-1}, which have been already assigned to formates. However, at temperatures higher than 200 °C new bands appeared at 1565, 1453, and 1309 cm^{-1}, increased in intensity with temperature. The bands at 1565 and 1453 cm^{-1} are attributed to the $\nu_{as}(COO^-)$ and $\nu_s(COO^-)$ of acetate species, respectively (see ref 16 and references therein). The band at 1309 cm^{-1} can be tentatively assigned to the out-of-plane bending mode of a $-CH_3$ fragment. A similar band was reported for the NO/C_3H_6 reaction over Rh/γ-Al_2O_3,[35] as well for Pd/γ-Al_2O_3 catalysts under simulated exhaust conditions.[36] The appearance of propane fragments and propane oxygenated species at temperatures higher than 200 °C indicates activation of propane at these temperatures. Given that propane oxidation occurs at temperatures practically higher than ca. 300 °C (Figures 1 and 2), this implies that consumption of propane proceeds through the decomposition of alkane (bands at 1309 cm^{-1}) and subsequently

TABLE 2: Surface Species and Their Peak Position in DRIFT Spectra

surface species	peak position (cm^{-1})	infrared vibration	references
bridging nitrate	1615	ν(N═O)	15, 29, 30
bidentate nitrate	1585	ν(N═O)	15, 29, 30
	1045	$\nu_s(NO_2)$	15, 29, 30
monodentate nitrate	1505	$\nu_{as}(NO_2)$	15, 29, 30
chelating nitro or bridging nitrite	1230	$\nu_s(NO_2)$	15, 29, 30
nitro compounds	1505	$\nu_{as}(NO_2)$	15, 29, 30
	1360	$\nu_{as}(NO_2)$	15, 29, 30
	1400	$\nu_{as}(NO_2)$	15, 29, 30
linear nitrosyl	1768	ν(N−O)	30
nitrate	2761	combination bands	29, 30
	2400		29, 30
nitro/nitrate	1313	$\nu_s(NO_2)$ or $\nu_{as}(NO_2)$	15, 29, 30
formates	1367	$\nu_s(COO^-)$	16 [and references therein]
	1392	δ(CH)	16 [and references therein]
	1586	$\nu_{as}(COO^-)$	16 [and references therein]
adsorbed hydrocarbon fragments	2870−3000	−CH stretching	16 [and references therein]
	1309	$-CH_3$ bending	35, 36
acetates	1453	$\nu_s(COO^-)$	16 [and references therein]
	1565	$\nu_{as}(COO^-)$	16 [and references therein]
isocyanates (NCO) on Al_2O_3	2235	ν(N═C═O)	16 [and references therein]

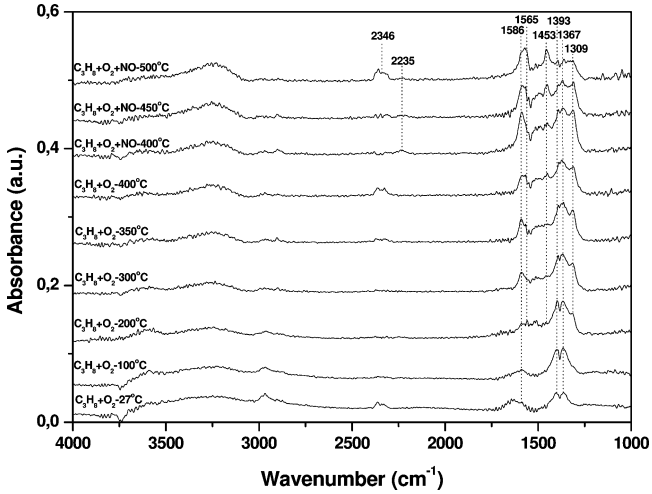

Figure 9. DRIFT spectra of Rh/Al_2O_3 at various temperatures under $C_3H_8 + O_2$ adsorption and during NO interaction with the $C_3H_8 + O_2$ gas mixture. FT-IR chamber feed: 1700 ppm C_3H_8 + 5% O_2 (+1300 ppm NO) in He; total flow rate = 80 cm^3/min.

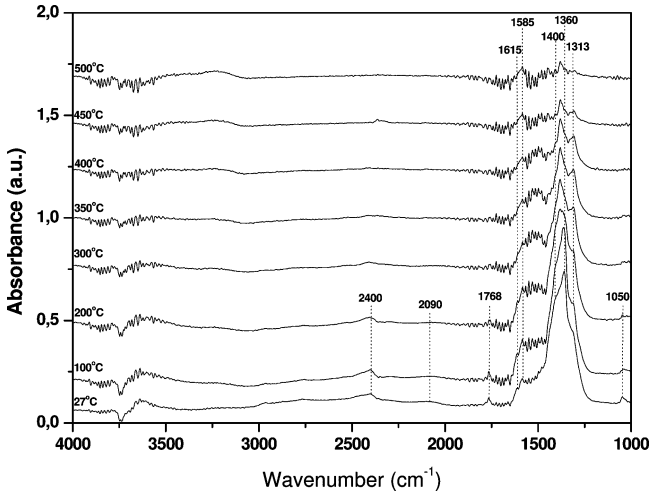

Figure 10. DRIFT spectra of Rh/Al_2O_3 at various temperatures under reaction conditions. FT-IR chamber feed: 1700 ppm C_3H_8 + 5% O_2 + 1300 ppm NO in He; total flow rate = 80 cm^3/min.

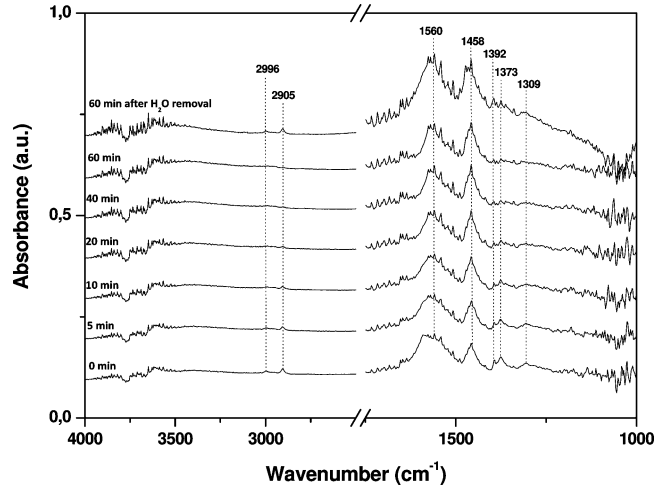

Figure 11. Time evolution of adsorbed species formed over Rh/Al_2O_3 at 410 °C during H_2O introduction to reaction feed stream. FT-IR chamber feed: 1700 ppm C_3H_8 + 5% O_2 + 1300 ppm NO + 3% H_2O in He; total flow rate = 80 cm^3/min.

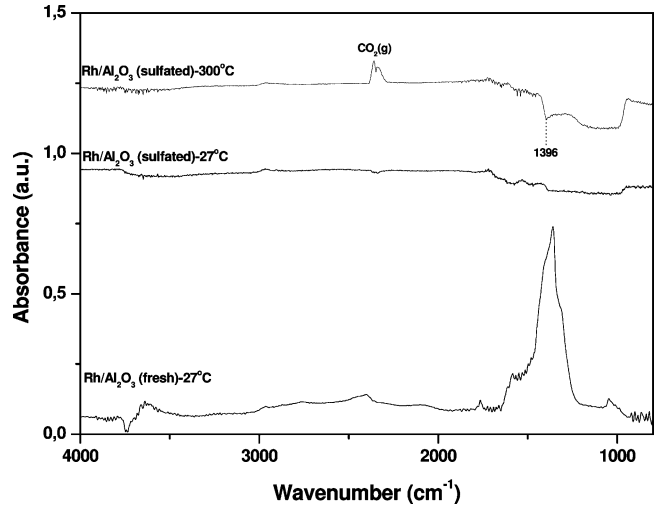

Figure 12. Comparison of DRIFT spectra obtained under reaction conditions over fresh and sulfated Rh/Al_2O_3 catalyst. FT-IR chamber feed: 1700 ppm C_3H_8 + 5% O_2 + 1300 ppm NO in He; total flow rate = 80 cm^3/min.

oxidation of its fragments to oxygenated species (formates, acetates). Addition of NO to $C_3H_8 + O_2$ flow at 400 °C results in the formation of weakly adsorbed isocyanates (band at 2235 cm^{-1}), whereas at the same time the intensity of carboxylate species (bands at 1586, 1453, 1393, 1367, 1309 cm^{-1}) is significantly increased. These findings are in a good agreement with those obtained by Eränen et al.[37] during the NO reduction by an alkane (octane) over $Ag/\gamma\text{-}Al_2O_3$ catalysts. On the basis of FTIR experiments, they concluded that NO is necessary for the formation of oxygenated species even in the presence of excess O_2, as it strongly participates as a reactant/oxidant in breaking the C−H bond, a step that could be rate-determining.[37]

Figure 10 shows the IR spectra acquired under reaction conditions over the 27−500 °C temperature range. Comparing the spectra under reaction conditions with the corresponding ones under NO + O_2 (Figure 7) and $C_3H_8 + O_2$ (Figure 8) conditions makes it obvious that, at temperatures lower than 300 °C, the catalysts surface is predominantly covered by nitrosyl (1768 cm^{-1}), carbonyl (2090 cm^{-1}), and nitro/nitrite (1300−1400 cm^{-1}) compounds. Bands due to carboxy species are not obvious as overlapped with the high intensity bands of NO_X ad-species. Increasing the temperature above 300 °C results in a significant decrease in the intensity of nitro/nitrite species as well as to the disappearance of nitrosyl and carbonyl species. Taking into account that during SCR, NO and propane conversions start at about 300 °C (Figures 1 and 2), this possibly indicates that NO, CO, and NO_2 ad-species are active intermediates. These findings are in accordance with the high reactivity of nitro/nitrite species toward CO and hydrocarbons.[16] At temperatures higher than 400 °C a significant attenuation of all bands is observed. The elimination of surface species at high temperatures is possibly consistent with the complete oxidation of propane and subsequently with the decrease of reductant efficiency (Figures 1 and 2).

Since the influence of H_2O and SO_2 was proven to be detrimental during the SCR of NO by C_3H_8, the next step was to investigate by means of IR spectroscopy the effect of these molecules on the surface chemistry, under exactly the same conditions imposed on stability experiments (Figures 3 and 4). Therefore, the influence of H_2O on IR spectra was in situ investigated by flowing the reaction mixture of NO + C_3H_8 + O_2 through a steam saturator so as to be enriched in H_2O (3%)

TABLE 3: Kinetic Parameters Obtained for the SCR of NO by C_3H_8 in the Absence/Presence of H_2O and SO_2

		$r = k[NO]^a[O_2]^b[C_3H_8]^c[H_2O]^d[SO_2]^e$				
	E_{act}(kcal/mol)	*a*	*b*	*c*	*d*	*e*
		NO Reduction				
absence of SO_2 and H_2O	29 ± 3.3	0.00 ± 0.02	0.47 ± 0.05	0.46 ± 0.05		
presence of H_2O	34 ± 2.5	0.94 ± 0.09	0.93 ± 0.08	0.47 ± 0.04	−1.52 ± 0.25	
presence of SO_2	52 ± 2.0	0.00 ± 0.03	0.53 ± 0.04	0.48 ± 0.02		−0.51 ± 0.06
		C_3H_8 Oxidation				
absence of SO_2 and H_2O	24 ± 2.0	0.00 ± 0.01	0.52 ± 0.03	0.49 ± 0.03		
presence of H_2O	25 ± 1.0	−0.46 ± 0.05	0.56 ± 0.08	0.55 ± 0.11	0.0 ± 0.01	
presence of SO_2	47 ± 1.7	0.00 ± 0.01	0.49 ± 0.06	0.51 ± 0.03		−0.54 ± 0.08

and then monitoring the spectra changes as a function of time. As depicted in Figure 11 before the introduction of H_2O on the IR cell, the catalyst's surface was predominantly covered by formates (1392, 1373 cm^{-1}), adsorbed hydrocarbons fragments (1309 cm^{-1}) and by acetates and/or NO_X ad-species characterized by the overlapping bands centered at 1560 and 1458 cm^{-1}. In the high frequency region the only observed bands are those at 2995 and 2905 cm^{-1}, attributed to hydrocarbon fragments and/or to alkyl groups associated with carboxylate species.[16] Interaction of H_2O molecules with the catalyst's surface results in a progressive decrease in intensity of the bands due to formates (1393, 1373 cm^{-1}) and hydrocarbon fragments (1309 cm^{-1}), which is consistent with the decrease in intensity of the high frequency bands at 2996 and 2905 cm^{-1}. In contrast, bands due to acetates and/or NO_X species remain almost unaffected over the whole period of H_2O interaction with catalyst. The present results indicate that the presence of water in the reaction feed stream significantly hinders the adsorption and consequently the activation of hydrocarbons, which in turn leads to the decrease of NO and C_3H_8 conversions under reaction conditions, as indeed observed (Figures 2 and 4). These findings are in accordance with the competition existing between water and hydrocarbon fragments for the same active sites.[22,25] It should be emphasized that water removal from the feed stream results in the reappearance of formates and hydrocarbon fragments, which is consistent with the reversible effect of H_2O on the C_3H_8 consumption rate (Figure 4).

The influence of SO_2 on the surface behavior of Rh/γ-Al_2O_3 catalyst was investigated by the IR spectra acquisition under reaction conditions over presulfated catalyst, i.e., catalyst treated ex situ for 24 h in a reaction mixture containing 300 ppm SO_2. This procedure was followed to avoid any damage effects of SO_2 on the IR cell. In Figure 12 the IR spectra obtained under reaction conditions (NO + C_3H_6 + O_2) over fresh and sulfated Rh/Al_2O_3 catalysts are depicted. It is evident that SO_2 treatment leads to the complete suppression of adsorbed species over both Rh and γ-Al_2O_3 sites, indicating the strong poison of catalyst's surface by sulfur species. In accordance with this assumption is the negative "plateau" in the region 1380−980 cm^{-1}, characteristic of sulfates on γ-Al_2O_3.[38] However, it should be noted that at higher temperatures (e.g., at 300 °C), the development of a negative band at 1390 cm^{-1} is observed, indicating the consumption of sulfated species;[23] at the same time the evolution of gas phase CO_2 is observed. This probably implies the participation of sulfated species on propane oxidation, justifying the enhanced oxidation activity of Rh/γ-Al_2O_3 catalysts after the removal of SO_2 from the feed stream (Figure 4).

3.4. Kinetic Analysis of NO_X Reduction and C_3H_8 Oxidation over Rh/Al_2O_3. Table 3 summarizes the results of kinetic studies that were performed to determine the apparent activation energies and reactants' partial reaction orders for NO reduction and C_3H_8 oxidation reactions in the absence and presence of SO_2 or H_2O. In this point it must be stated that kinetic studies were carried out at reaction conditions ensuring the reactor's differential operation, based on preliminary experiments concerning the influence of particle size and W/F ratio on catalytic activity. To this end, a W/F value of 0.12 g s/cm^3 and samples with particle sizes in the range 180−355 μm were selected for the intrinsic kinetic measurements. The calculation of apparent activation energies was performed in the temperature interval of 325−370 °C with a reacting mixture consisting of: NO (0.13%), O_2 (5%), C_3H_8 (0.17%); when H_2O or SO_2 was used, their concentrations were kept constant to 3% and 50 ppm, respectively. Apparent reaction orders were estimated at low conversion conditions (T < 345 °C) by varying reactants concentrations as follows: NO (0.03−0.27%), O_2 (1.9−7%), C_3H_8 (0.25−0.65%), H_2O (1.9−3%), SO_2 (0.015−0.5%).

Combining the estimated kinetic parameters listed in Table 3 yielded the following overall low-T power law kinetic expressions for the NO reduction and C_3H_8 oxidation reactions over Rh/γ-Al_2O_3 in the absence of H_2O and SO_2:

$$r_{red} = [O_2]^{0.5}[C_3H_8]^{0.5} \quad (1)$$

$$r_{ox} = [O_2]^{0.5}[C_3H_8]^{0.5} \quad (2)$$

The identical low-T kinetics (eqs 1 and 2) and the similar apparent activation energies (29 and 24 kcal/mol for NO reduction and propane oxidation reactions, respectively), imply a common rate determining step (rds) for both processes. In other words, the NO reduction is directly linked with the activation of the reductant. On the basis of this observation and on IR results, it could be suggested that C_3H_8 via its fragmental species participates in the reduction of Rh sites, which are considered as the active sites for NO reduction.[17]

The zero-order dependence of both kinetic expressions from NO indicates that NO is not participating in the rds. This assumption is consistent with a "reduction" type mechanism, where the rds is most probably related with the formation of active carboxylates ($C_xH_yO_z$) through the interaction of hydrocarbon fragmental species with O_{ad} species generated from the dissociative adsorption of gas phase O_2 and/or NO. In addition, this zero-order dependence cannot be assigned to either the formation of NO_X or the reaction between them and the carboxylates, since in such a case NO would appear in the kinetic expressions. This explanation is in accordance with the corresponding findings in the NO + O_2 + C_3H_8-TPD experiment over Rh/γ-Al_2O_3, where it was observed that the NO_X species that desorbed at the high temperature peak were significantly decreased compared to the NO + O_2-TPD, due to their quick consumption by the carboxylate species.

As a consequence, the positive half-order dependence of O_2 implies its activation through dissociative adsorption; it is possible that O_{ad} participates to the formation of active intermediate species such as $C_xH_yO_z$, as indeed detected in DRIFTS experiments. The fractional order dependence of kinetic expressions from propane, possibly implies the participation of propane derived species on the rds. Its positive role can be attributed to the formation of active intermediates such as formates and acetates, as well as to the reduction of Rh active sites leading to the enhancement of NO reduction.[17]

Similar experiments were carried out by Nikolopoulos et al.[11] to investigate the kinetics of the C_3H_6-SCR of NO in excess oxygen over 1.86% Rh/γ-Al_2O_3. The estimated apparent activation energies were higher compared to the present ones (36 and 38 kcal/mol for NO reduction and propene oxidation reactions, respectively), indicating the significant role of hydrocarbon on the SCR. In a similar kinetic study of NO SCR by C_3H_6 over 2% In/Al_2O_3 a similar activation energy for C_3H_6 oxidation was found (33 kcal/mol) whereas the apparent activation energy for NO reduction was significantly lower (8.7 kcal/mol), implying the crucial role of metal nature on NO adsorption, which is considered as the rds for NO reduction.[22]

As far as the reaction order is concerned, in the work of Nikolopoulos et al.[11] over Rh/γ-Al_2O_3, a half-order dependence on O_2 was observed for both reactions, while C_3H_6 did not appeared in rate expressions. Only in the case of the propene oxidation kinetic expression was a first-order negative dependence on NO determined.[11] On the basis of these observations, a reaction mechanism was proposed, in which the rds involves the interaction between propene intermediate species and oxygen ad-atoms.[11]

3.4.1. Effect of H_2O on the Kinetics. In the presence of H_2O and taking into account the experimental error (Table 3), the following low-*T* kinetic expressions could be obtained:

$$r_{red} = \frac{[NO][O_2][C_3H_8]^{0.5}}{[H_2O]^{1.5}} \quad (3)$$

$$r_{ox} = \frac{[O_2]^{0.5}[C_3H_8]^{0.5}}{[NO]^{0.5}} \quad (4)$$

By comparing the above rate expressions with the corresponding ones in the absence of H_2O (eqs 1 and 2), one should argue that the reaction mechanism underlies a few changes in the presence of water. Furthermore, comparing eqs 3 and 4 and taking into account the different apparent activation energies of the corresponding reactions (34 kcal/mol for NO reduction and 25 kcal/mol for propane oxidation, respectively) seem to indicate that the rds for NO reduction is different from the elementary step that determines the propane oxidation reaction rate.

The first-order dependence of NO reduction by O_2 implies the direct participation of gas phase oxygen in the formation of active intermediates. Taking into account the corresponding TPD experiments (section 3.2), where it was found that the presence of H_2O suppresses the desorbed amount of NO_X ad-species, this implies the key role of O_2 under hydrated conditions on the formation of NO_X intermediates. As a consequence, the positive first-order dependence of NO can be assigned to the participation of nitrosyl species or gas phase NO to the formation of NO_X. However, it cannot be excluded that NO may interact from gas phase with other intermediate species (mainly carboxylates or isocyanates) to generate the final products, a step which also justifies the first-order dependence on NO. This specific step is further supported by DRIFTS results where it was found that the reaction products could be the result of NO interaction with active intermediates, such as isocyanates ($-$NCO).

The negative order dependence of NO reduction by water denotes that its presence hinders the reaction rate, as indeed found on activity (Figure 2) and stability (Figure 4) experiments. This specific inhibition can be attributed, on the basis of TPD and FTIR studies, to competitive adsorption between H_2O and other reactants as well as to the oxidation of Rh sites,[24] which in turn hinders the NO dissociative adsorption.

In the case of propane oxidation reaction based on the same apparent activation energies and the quite similar rate expressions in the absence and presence of H_2O, it can be stated that the mechanism of C_3H_8 activation is not significantly affected by water, although its adsorption is hindered by water, as observed in the IR-spectra (Figure 11). Water seems to affect only the adsorption of propane and not its combustion mechanism; this is consistent with the reversible effect of water on propane conversion (Figure 4). The negative half-order dependence of NO can be attributed to the competition existing, under hydrated conditions, between NO_{ad} and C_3H_8 or propane-derived species for the same active sites responsible for propane oxidation.

3.4.2. Effect of SO_2 on the Kinetics. The presence of SO_2 results in the following low-T kinetic rate expressions:

$$r_{red} = \frac{[O_2]^{0.5}[C_3H_8]^{0.5}}{[SO_2]^{0.5}} \quad (5)$$

$$r_{ox} = \frac{[O_2]^{0.5}[C_3H_8]^{0.5}}{[SO_2]^{0.5}} \quad (6)$$

The coincide rate expressions (eqs 5 and 6) as well as the similar apparent activation energies (52 and 47 kcal/mol, respectively) lead to the conclusion that both processes are determined by a similar elementary step, which seems to be the same as in the absence of SO_2. The negative half-order dependence of SO_2 on both processes' kinetics indicates its inhibiting role, as indeed observed in activity (Figure 1) and stability (Figure 3) experiments. This inhibition has been already assigned to the catalyst's surface poisoning by sulfate compounds, which in turn hinders the adsorption ability.

Rarely, similar studies are encountered in the related literature, concerning the investigation of HC-SCR kinetics in the presence of H_2O and SO_2. Marnellos et al.[22] have performed similar experiments in the copresence of both poisonous gases over In/γ-Al_2O_3; it was found that the corresponding activation energies were remained essentially the same as in the absence of SO_2 and H_2O, while the reactants' reaction orders were accordingly modified, implying a different reaction pathway when the poisonous gases are present in the feed.[22]

3.5. Proposed Reaction Mechanism. In this point, on the basis of the present DRIFTS, TPD, and kinetic studies, a possible mechanistic scheme for the C_3H_8-SCR of NO over Rh/γ-Al_2O_3 catalyst will be proposed. It should be noted, however, that due to the complexity of the process it is very difficult to establish a generally accepted reaction mechanism, as already has been mentioned in the literature (e.g., refs 3 and 39). Nevertheless, taking into account the results emerged from kinetic and mostly the surface studies, we have some evidence

that SCR of NO by C_3H_8 under lean conditions, could be proceed through the following steps:

1. Formation of nitrosyls over Rh sites, which in turn could lead to NO molecules decomposition to N- and O- adsorbed atoms. This step is consistent with the high dissociation activity of Rh entities.

2. Formation of nitroxy species (NO_X ad-species) via interaction of N- and O-containing species with the acid sites of the support.

3. Formation of oxygenated hydrocarbon species via interaction of adsorbed hydrocarbon fragments with O_{ad} species generated from the dissociative adsorption of gas phase O_2 and/or NO; this specific step is considered as the rds.

4. Formation of isocyanate species (−NCO) possibly via interaction of oxygenated hydrocarbon species with either gas phase NO or NO_X ad-species.

5. Formation of reaction products through the interaction of isocyanates with NO + O_2 from gas phase and/or NO_X ad-species.

A similar reaction scheme has been proposed by Mosqueda-Jimenez et al.[40] during the NO reduction by octane over Ni-based catalysts. In accordance with the authors, initially nitrates and nitro species formed on the catalyst's surface are transformed to organic nitro/nitrito species in the presence of alkane. The latter species are considered as the precursors of isocyanate species, which finally react with NO_2 from the gas phase to yield N_2. Moreover, He et al.[42] on the basis of in situ FTIR studies suggest that SCR of NO by C_3H_8 over Co/Al_2O_3 catalysts starts with partial oxidation of propane to adsorbed carboxylates. These as-formed carboxylates act as an effective reductant for NO reduction. In addition, NO_X ad-species are reactive to propane and oxygenates, whereas NCO species are considered as active intermediates in the formation of N_2.[41] The significant role of NO_X ad-species and carboxylates as active intermediates during SCR of NO has been also mentioned by Shimizu et al.[42]

Concerning the effect of H_2O, it could be argued on the basis of the present work that water molecules affect to a different extent the NO reduction and C_3H_8 oxidation reactions. In relation to NO reduction, it was found that H_2O competes with other reactants for the same active sites, thus decreasing the adsorption of NO_X ad-species and consequently the activation of NO. In addition, the oxidation of Rh sites by water is considered to be responsible for the irreversible effect of H_2O on NO reduction (Figure 4). On the other hand, the reversible negative effect of H_2O on C_3H_8 oxidation can be solely attributed to competitive adsorption, an assumption verified by IR (Figure 11) and stability (Figure 4) studies. In SO_2-containing feed mixtures the reaction mechanism is similar to that described in the case of the ideal reacting mixture. However, SO_2 has a clear irreversible poisoning effect on the overall catalytic performance, attributed to the formation of strongly adsorbed sulfate compounds that hinder the adsorption of reactants. The effect is stronger for NO reduction, while in the case of propane oxidation the inhibition is milder due to the participation of sulphated species on C_3H_8 oxidation.

4. Conclusions

In the present work the surface and catalytic behavior of Rh/γ-Al_2O_3 catalysts were explored during the selective reduction of NO by C_3H_8 in the presence of excess oxygen, H_2O and SO_2. Particular emphasis was given to the identification of the elementary steps that describe the reaction mechanism under ideal and nonideal reaction conditions. Activity and stability tests as well as TPD studies in combination with in situ DRIFTS measurements were carried out at various reaction conditions to correlate the catalytic performance of Rh/γ-Al_2O_3 catalysts with its corresponding surface chemistry. Results revealed that in the absence of H_2O and SO_2, the reaction follows a typical "reduction" type mechanism, where the active intermediates (NO_X, carboxylates, isocyanates) are interacting to yield the final products. In the reaction sequence that was proposed, the rate determining step (rds) is the formation of $C_xH_yO_z$ species originating from the partial oxidation of C_3H_8 fragmental species. Water addition to the reaction mixture significantly suppresses the overall conversion performance of Rh/Al_2O_3 catalyst. Its inhibiting effect was totally reversible in the case of C_3H_8 oxidation, whereas the NO reduction reaction was permanently affected due to the oxidation of Rh sites, which are considered as the active sites for NO reduction. In contrast, SO_2 inhibited both reactions irreversibly due to the formation of surface sulfates, which hinders the adsorption and consequently the activation of reactants.

Acknowledgment. The present research was cofunded from the European Union (ESF) by 75% and the Hellenic State by 25% through the Operational Programme Competitiveness PENED 2003 [03 ED 940].

References and Notes

(1) Roy, S.; Hedge, M. S.; Madras, G. *Appl. Energy* **2009**, *86*, 2283.
(2) Kaspar, J.; Fornasiero, P.; Hickey, N. *Catal. Today* **2003**, *77*, 419.
(3) Burch, R.; Breen, J. P.; Meunier, F. C. *Appl. Catal., B* **2002**, *39*, 283.
(4) Parvulescu, V. I.; Grange, P.; Delmon, B. *Catal. Today* **2002**, *39*, 283.
(5) Traa, Y.; Burger, B.; Weitkamp, J. *Microporous Mesoporous Mater.* **1999**, *30*, 3.
(6) Praserthdam, P.; Chaisuk, C.; Panit, A.; Kraiwattanawong, K. *Appl. Catal., B* **2002**, *38*, 227.
(7) Iwamoto, M.; Furukawa, H.; Mine, Y.; Uemura, F.; Mikuriya, S.; Kagawa, S. *J. Chem. Soc., Chem. Commun.* **1986**, 1272.
(8) Sparks, D. E.; Patterson, P. M.; Jacobs, G.; Dogimont, N.; Tackett, A.; Crocker, M. *Appl. Catal., B* **2006**, *65*, 44.
(9) Kung, M. C.; Park, P. W.; Kim, D. W.; Kung, H. H. *J. Catal.* **1999**, *181*, 1.
(10) Meunier, F. C.; Ukropec, R.; Stapleton, C.; Ross, J. R. H. *Appl. Catal., B* **2001**, *30*, 163.
(11) Nikolopoulos, A. A.; Stergioula, E. S.; Efthmiadis, E. A.; Vasalos, I. A. *Catal. Today* **1999**, *54*, 439.
(12) Kotsifa, A.; Kondarides, D. I.; Verykios, X. E. *Appl. Catal., B* **2008**, *80*, 260.
(13) Burch, R.; Millington, P. J. *Catal. Today* **1995**, *26*, 185.
(14) Amiridis, M. D.; Mihut, C.; Maciejewski, M.; Baiker, A. *Top. Catal.* **2004**, *28*, 141.
(15) Koukiou, S.; Konsolakis, M.; Lambert, R. M.; Yentekakis, I. V. *Appl. Catal., B* **2007**, *76*, 101.
(16) Matsouka, V.; Konsolakis, M.; Lambert, R. M.; Yentekakis, I. V. *Appl. Catal., B* **2008**, *84*, 715.
(17) Long, R. Q.; Yang, R. T. *J. Phys. Chem. B* **1999**, *103*, 2232.
(18) Halkides, T. I.; Kondarides, D. I.; Verykios, X. E. *Catal. Today* **2002**, *73*, 213.
(19) Vernoux, P.; Gaillard, F.; Bultel, L.; Siebert, E.; Primet, M. *J. Catal.* **2002**, *208*, 412.
(20) Burch, R.; Crittle, D. J.; Hayes, M. J. *Catal. Today* **1999**, *47*, 229.
(21) Burch, R.; Watling, T. C. *Catal. Today* **1997**, *43*, 19.
(22) Marnellos, G. E.; Efthimiadis, E. A.; Vasalos, I. A. *Appl. Catal., B* **2004**, *48*, 1.
(23) Efthimiadis, E. A.; Christoforou, S. C.; Nikolopoulos, A. A.; Vasalos, I. A. *Appl. Catal., B* **1999**, *22*, 91.
(24) Kiss, J.; Solymosi, F. *Surf. Sci.* **1986**, *177*, 191.
(25) Efthimiadis, E. A.; Lionta, G. D.; Christoforou, S. C.; Vasalos, I. A. *Catal. Today* **1998**, *40*, 15.
(26) Miyahara, Y.; Takahashi, M.; Masuda, T.; Imamura, S.; Kanai, H.; Iwamoto, S.; Watanabe, T.; Inoue, M. *Appl. Catal., B* **2008**, *84*, 289.
(27) Kotsifa, A.; Kondarides, D. I.; Verykios, X. E. *Appl. Catal., B* **2007**, *72*, 136.
(28) Burch, R.; Sullivan, J. A.; Watling, T. C. *Catal. Today* **1998**, *42*, 13.
(29) Venkov, T.; Hadjivanov, K.; Klissurski, D. *Phys. Chem. Chem. Phys.* **2002**, *4*, 2443.

(30) Hadjiivanov, K. I. *Catal. Rev.-Sci. Eng.* **2000**, *42*, 71.
(31) Szanyi, J.; Kwak, J. H.; Chimentao, R. J.; Peden, C. H. F. *J. Phys. Chem. C* **2007**, *111*, 2661.
(32) Ingelsten, H. H.; Hildesson, A.; Fridell, E.; Skoglundh, M. *J. Mol. Catal. A* **2004**, *209*, 199.
(33) Flores-Moreno, J. L.; Delahay, G.; Fiquers, F.; Coq, B. *J. Catal.* **2005**, *236*, 292.
(34) Li, J.; Ke, R.; Hao, J. *Catal. Today* **2008**, *139*, 49.
(35) Anderson, J. A.; Rochester, C. H. *J. Chem. Soc., Faraday Trans.* **1989**, *85*, 1117.
(36) Martínez-Arias, A.; Fernández.-Garcia, M.; Hungría, A. B.; Iglesias-Juez, A.; Duncan, K.; Smith, R.; Anderson, J. A.; Conesa, J. C.; Soria, J. *J. Catal.* **2001**, *204*, 238.
(37) Eränen, K.; Lindfors, L.-E.; Klingstedt, F.; Murzin, D. Y. *J. Catal.* **2003**, *219*, 25.
(38) Chang, C. C. *J. Catal.* **1978**, *53*, 374.
(39) He, Ch.; Paulus, M.; Find, J.; Nickl, J. A.; Eberle, H.-J.; Spengler, J.; Chu, W.; Köhler, K. *J. Phys. Chem. B* **2005**, *109*, 15906.
(40) Mosqueda-Jiménez, B. I.; Jentys, A.; Seshan, K.; Lercher, J. A. *Appl. Catal., B* **2003**, *46*, 189.
(41) He, Ch.; Köhler, K. *Phys. Chem. Chem. Phys.* **2006**, *8*, 898.
(42) Shimizu, K.-I.; Shibata, J.; Yoshida, H.; Satsuma, A.; Hattori, T. *Appl. Catal., B* **2001**, *30*, 151.

JP907589C